Acta Cryst. (1991). B47, 305–314

Structure Determinations for $Ca_3Ti_2O_7$, $Ca_4Ti_3O_{10}$, $Ca_{3.6}Sr_{0.4}Ti_3O_{10}$ and a Refinement of $Sr_3Ti_2O_7$

BY M. M. ELCOMBE AND E. H. KISI*

Australian Nuclear Science and Technology Organisation, Private Mailbag 1, *Menai, NSW* 2234, *Australia*

K. D. HAWKINS AND T. J. WHITE

Electron Microscope Centre, University of Queensland, St Lucia, QLD 4067, *Australia*

AND P. GOODMAN AND S. MATHESON

School of Physics, University of Melbourne, Parkville, VIC 3052, *Australia*

(*Received* 6 *July* 1990; *accepted* 26 *November* 1990)

Abstract

The structures of the orthorhombic Ruddlesden–Popper ($A_{n+1}B_nX_{3n+1}$) phases $Ca_3Ti_2O_7$ ($n=2$) [M_r = 328·04, $Ccm2_1$, a = 5·4172 (1), b = 19·5169 (4), c = 5·4234 (1) Å, V = 573·40 Å^3, Z = 4, D_x = 3·80 g cm^{-3}, R_B = 1·37%], $Ca_4Ti_3O_{10}$ ($n=3$) [M_r = 464·02, $Pcab$, a = 5·4083 (1), b = 27·1432 (4), c = 5·4337 (1) Å, V = 797·66 Å^3, Z = 4, D_x = 3·86 g cm^{-3}, R_B = 1·53%] and $Ca_{3.6}Sr_{0.4}Ti_3O_{10}$ (n = 3) [M_r = 483·04, $Pcab$, a = 5·4409, b = 27·2727 (7), c = 5·4415 (2) Å, V = 807·45 Å^3, Z = 4, D_x = 3·97 g cm^{-3}, R_B = 1·55%] have been determined, and that of tetragonal $Sr_3Ti_2O_7$ [M_r = 470·66, $I4/mmm$, a = 3·9026 (1), c = 20·3716 (4) Å, V = 310·27 Å^3, Z = 2, D_x = 5·55 g cm^{-3}, R_B = 1·54%] refined from neutron powder diffraction data at λ = 1·893 Å. They consist of coherent intergrowths of perovskite ($CaTiO_3$) blocks, n TiO_6 octahedra thick, with single layers of CaO having a distorted NaCl configuration. TiO_6 octahedra are tilted and distorted in a very similar fashion to those in $CaTiO_3$ ($n = \infty$). This fact was used to determine the space groups of the layered structures. Convergent-beam electron diffraction patterns are best matched by calculations in the above space groups which are thus confirmed. Octahedral tilt angles increase slightly in the sequence n = 2, 3, ∞. Strontium addition reduces the octahedral tilt angles because of preferential substitution of Sr on the Ca sites within the perovskite blocks of $Ca_4Ti_3O_{10}$. The algorithm used to produce starting models for structure refinements is thought to be generally applicable to Ruddlesden–Popper and possibly other layered perovskite structures. It furnishes the predictions: (*a*) all n-even compounds in the $Ca_{n+1}Ti_nO_{3n+1}$ series will have space group $Ccm2_1$, (*b*) all n-odd compounds in this series will have space group $Pcab$, (*c*) all $A_{n+1}B_nX_{3n+1}$ series for which the $n = \infty$ end member (ABX_3) is isostructural with $CaTiO_3$ will be isostructural with the compounds reported above (*e.g.* $Ca_{n+1}Zr_nO_{3n+1}$).

1. Introduction

Compounds with the formula ABX_3, where A and B are metal cations and X is oxygen or one of the halides, often crystallize in perovskite structures. Perovskites form the basis for several polysomatic series. One group of such structures is known as the Ruddlesden–Popper phases and conforms to the generic formula $A_{n+1}B_nX_{3n+1}$ [$=n(ABX_3).AX$]. Chemically they are perovskites containing an excess of A cations which structurally are accommodated by the regular insertion of distorted NaCl-type layers intergrown with perovskite blocks. The value of n equates with the number of layers of corner-sharing BX_6 octahedra in each perovskite block.

Ruddlesden & Popper (1957, 1958) described the series Sr_2TiO_4 (n = 1), $Sr_3Ti_2O_7$ (n = 2) and $Sr_4Ti_3O_{10}$ (n = 3), and recognized their structures as higher-order polytypes of the K_2NiF_4 structure type from X-ray powder diffraction photographs. Independently of this Dry's & Trzebiatowski (1957) reported the phase equilibria and Lukaszewicz (1959) the structures of these SrO–TiO_2 phases. Ruddlesden & Popper postulated atom positions in the space group $I4/mmm$ (No. 139) and calculated intensities which were in excellent agreement with the observed patterns. The a and b unit-cell parameters are approximately equal to the cubic cell parameter of the $SrTiO_3$ ($n = \infty$) end member. In this SrO–TiO_2 series the TiO_6 octahedra have their fourfold axes aligned with the unit-cell edges.

$CaTiO_3$ has TiO_6 octahedra which are tilted with respect to cubic perovskite axes. The symmetry is

* Now at Division of Science and Technology, Griffith University, Nathan, QLD 4111, Australia.

0108-7681/91/030305-10$03.00

reduced to orthorhombic, space group *Pcmn* (No. 62), with unit-cell parameters approximately related to the pseudo-cubic subcell as: $a_o \simeq \sqrt{2}a_c$, $b_o \simeq 2a_c$, $c_o \simeq \sqrt{2}a_c$. Roth (1958), Kwestroo & Paping (1959) and Tilloca & Perez y Jorba (1964) reported the existence of Ruddlesden–Popper phases with $n = 2$ and $n = 3$ in the CaO–TiO_2 system. Tilloca & Perez y Jorba determined the symmetry of their structures to be orthorhombic. The space-group symmetry and atom coordinates were not determined.

In this paper the refined coordinates of $CaTiO_3$ presented by Koopmans, van de Velde & Gellings (1983) are used to deduce the structures of $Ca_3Ti_2O_7$, $Ca_4Ti_3O_{10}$ and $Ca_{3.6}Sr_{0.4}Ti_3O_{10}$. These structures are confirmed and refined from neutron powder diffraction data and are shown to be consistent with convergent-beam electron diffraction (CBED) patterns. A refinement of the $Sr_3Ti_2O_7$ structure is also presented which confirms the structure proposed by Ruddlesden & Popper (1958).

2. Experimental

The compounds $Sr_3Ti_2O_7$, $Ca_3Ti_2O_7$, $Ca_4Ti_3O_{10}$ and $Ca_{3.4}Sr_{0.6}Ti_3O_{10}$ were synthesized from stoichiometric quantities of TiO_2, $CaCO_3$ and $SrCO_3$. Powders were mixed for 5 min in a laboratory tungsten carbide ball mill and calcined for 1 h at 1173 K in air, followed by grinding to -74 μm. Pellets (13 mm diameter × 2·5 mm) were pressed at 1300 Pa for 7 min and subsequently fired at 1773 K for 72 h and a further 120 h after crushing and resizing.

X-ray powder diffraction was used for initial sample characterization and showed that the $n = 3$ samples contained some of the $n = 2$ phase and the $Sr_3Ti_2O_7$ sample some $SrTiO_3$. The $Ca_3Ti_2O_7$ sample was single phase. Neutron data were collected on the high-resolution powder diffractometer HRPD (Howard, Ball, Davis & Elcombe, 1983) at the Australian Nuclear Science and Technology Organisation's HIFAR reactor. A neutron wavelength of 1·893 (1) Å was used to record scans from 10 to 160° of 2θ in 0·05° steps. Samples were contained in 12 mm diameter vanadium cans and rotated during data collection.

3. Space-group symmetry

3.1. $n = 2$

Gaussian functions were fitted to 92 peaks in the $Ca_3Ti_2O_7$ neutron diffraction pattern.* Peak positions were corrected for counter zero error and peak asymmetry. Indexing and unit-cell refinement gave the parameters $a = 5{\cdot}4172$ (1), $b = 19{\cdot}5169$ (4), $c = 5{\cdot}4234$ (1) Å. Determination of the reflection conditions was made difficult by the near equality of a and c. However, analysis of the peak half-widths showed most to be of instrumental width; hence unambiguous indexing could be established for most reflections. The reflection conditions hkl: $h + k = 2n$, $h00$: $h = 2n$, $0k0$: $k = 2n$, $00l$: $l = 2n$, $h0l$: h or l or both $= 2n$, $hk0$: $h + k = 2n$, $0kl$: k or l or both $= 2n$, were deduced with lowest confidence in the latter three. The most probable space groups from this analysis are therefore $Ccm2_1$ (No. 36), *Ccmm* (No. 63) and $C222_1$ (No. 20).

Because $CaTiO_3$ is a member of the series $Ca_{n+1}Ti_nO_{3n+1}$ (with $n = \infty$), it was considered likely that the tilts in the lower-order members would have the same sense and similar magnitudes to those in $CaTiO_3$. Consequently, a model for $Ca_3Ti_2O_7$ was deduced by introducing the relative atom positions

* Lists of bond lengths and observed step-scan neutron diffraction data have been deposited with the British Library Document Supply Centre as Supplementary Publication No. SUP 53730 (19 pp.). Copies may be obtained through The Technical Editor, International Union of Crystallography, 5 Abbey Square, Chester CH1 2HU, England.

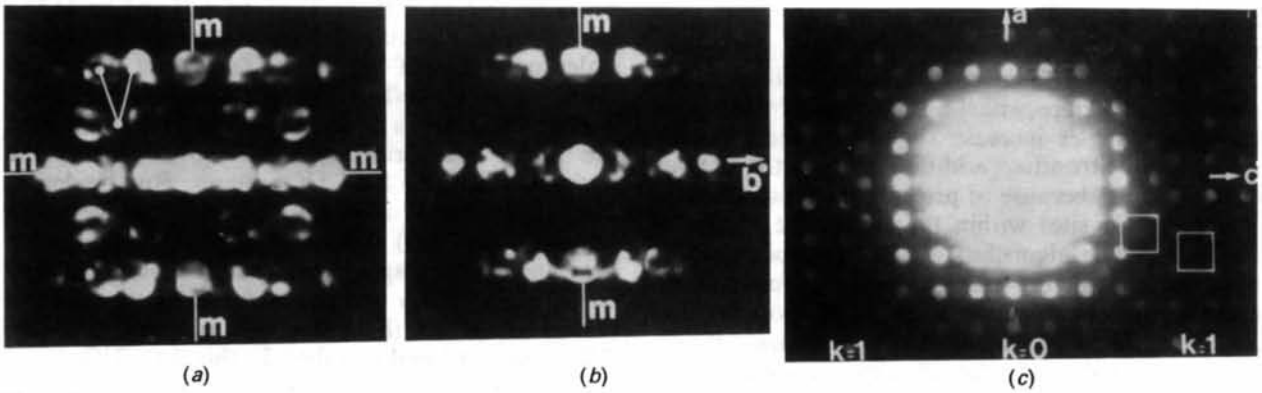

(*a*) (*b*) (*c*)

Fig. 1. Convergent-beam electron diffraction (CBED) patterns from the [100], [001] and [010] zones of $Ca_3Ti_2O_7$. The [100] zone (*a*) has *cmm* symmetry. The weak reflections along the $l = 2n$ rows are present and centred according to $k + l = 2n$. The [001] zone (*b*) has no mirror symmetry across b^* and consequently has *pm*1 symmetry, with $h = 2n$ rows absent. In the [010] zone pattern (*c*), $l = 2n$ for $h = 0$ in the zero-order Laue zone.

of a double perovskite block from $CaTiO_3$ into the unit cell of $Ca_3Ti_2O_7$ in an analogous way to the double perovskite block (of $SrTiO_3$) in $Sr_3Ti_2O_7$. A *C*-face centring was used to generate the second double perovskite block (equivalent to the body-centring of tetragonal $Sr_3Ti_2O_7$). The symmetry of the resultant collection of atoms conforms to the space group $Ccm2_1$, consistent with the observed systematic absences.

The [100] and [001] zero-layer CBED patterns are shown in Figs. 1(*a*) and 1(*b*). The projection symmetries of these patterns are *cmm* and *pm*1 respectively. This combination of symmetries in the orthorhombic system allows only the face-centred space groups $Ccm2_1$ (No. 36) and *Ccc*2 (No. 37), and the body-centred space groups *Iba*2 (No. 45) and *Ima*2 (No. 46).

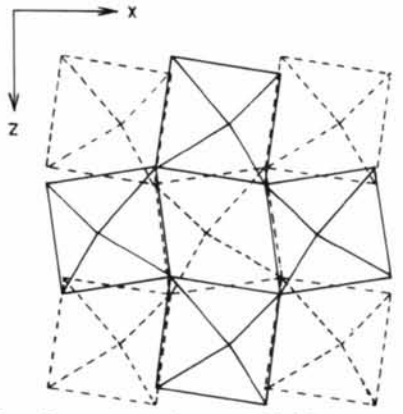

Fig. 2. The interface structure between adjoining perovskite blocks viewed down the *y* axis. The bottom halves of upper octahedra are drawn solid and the upper halves of octahedra in the block below are drawn dashed.

Table 1. *Zone observations from* $Ca_3Ti_2O_7$

	[001] *hk*0	[100] 0*kl*	[010] *h*0*l*
Symmetry	*cmm*	*pm*1 or *pg*1	Undetermined
Absences	$h + k = 2n$	$l = 2n$; $k = 2n$	$00l$; $l = 2n$; $h0l$; $l = 2n$

Complete determination of the space group depends on analysis of patterns from the [010] zone axis. These were difficult to obtain owing to a preferential cleavage along planes parallel to [010]. Those obtained were featureless disk (thin-crystal) patterns which could not be aligned precisely and so the projection symmetry was not determined. However, the long projection axis allows clear observation of the lattice extinctions in the higher-order Laue zone ($k = 1$). Extinction conditions from Fig. 1(*c*) are: $h0l$: $h = 2n$, ($l = 2n$?), $h1l$: $h = 2n + 1$, $l = 2n + 1$, leaving the conditions $h + k$, $k + l$, $l + h = 2n$. This observation rules out the body-centred space groups ($h + k + l = 2n$) and leaves only $Ccm2_1$ and *Ccc*2.

Distinction between $Ccm2_1$ and *Ccc*2 rests on whether the $l = 2n + 1$ reflections are (*a*) absent only along the central row ($h = 0$) or (*b*) absent generally over the whole zero layer. Condition (*a*) better describes the pattern although the *l*-odd reflections are everywhere weak. This favours $Ccm2_1$ in agreement with the neutron diffraction analysis. A summary of the CBED data is given in Table 1.

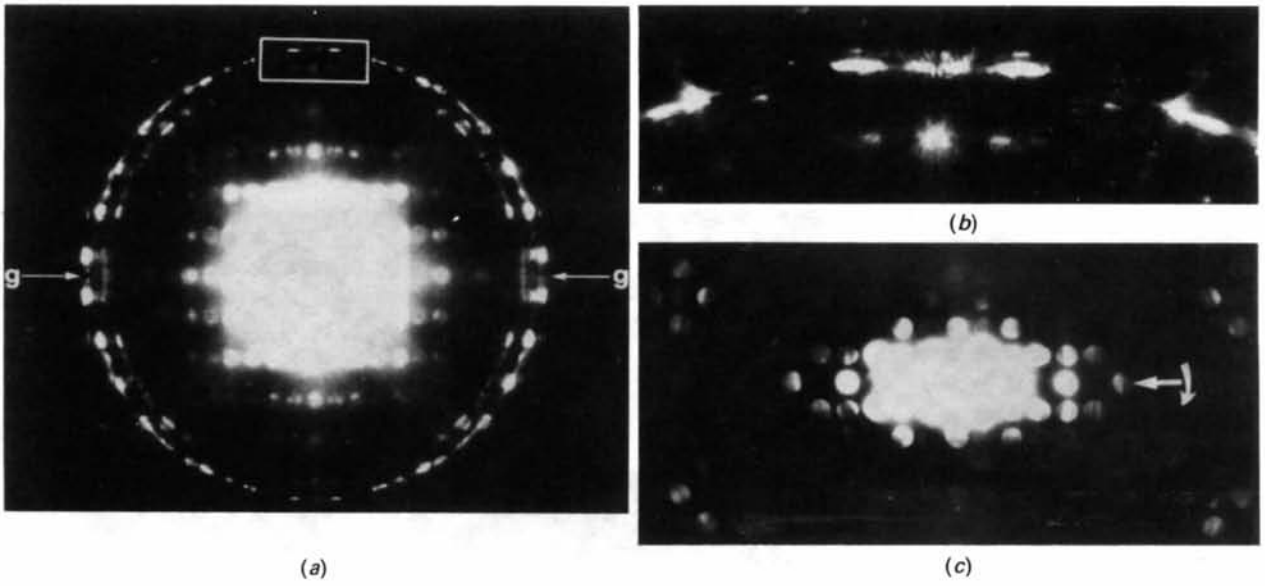

Fig. 3. (*a*) CBED pattern from the [010] zone axis of $Ca_4Ti_3O_{10}$. Arrows indicate extinction bands through first-order Laue zone and zero-layer reflections having *h* odd. (*b*) Enlargement of the boxed region of (*a*) showing an extinction band through the 101 first-order reflection. (*c*) CBED pattern from the [041] zone axis of $Ca_4Ti_3O_{10}$ showing complete extinction of the (*h*00) *h*-odd reflections. The arrow directed along the a^* axis indicates both the rotation from the [010] zone axis and the direction of the deduced 2_1 screw axis.

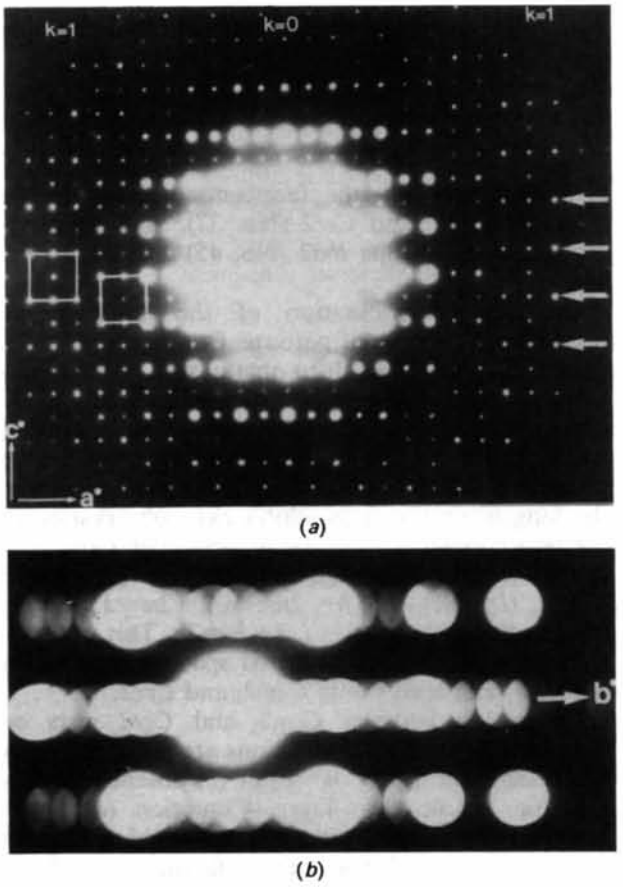

Fig. 4. (*a*) Point diffraction pattern from the [010] zone axis of $Ca_4Ti_3O_{10}$ showing the characteristic *l*-odd absent (very weak) at the centre of the pattern ($k = 0$) change to *l*-odd strong in the first-order Laue zone ($k = 1$). The strong reflections (11,1,1), (11,1,3), (11,1,$\bar{1}$), (11,1,$\bar{3}$) are arrowed for comparison with calculations. (*b*) Part of the [101] CBED pattern from $Ca_4Ti_3O_{10}$. The central row shows systematic extinction of *k*-odd reflections. In other rows, many *k*-odd reflections are observed.

The $Sr_3Ti_2O_7$ neutron pattern indexed directly to the tetragonal cell $a = 3{\cdot}9026\,(1)$, $c = 20{\cdot}3716\,(4)$ Å and gave no indication of deviation from *I*4/*mmm* symmetry. This was confirmed by CBED.

3.2. $n = 3$

A similar model-building approach as that used for $Ca_3Ti_2O_7$ was applied to $Ca_4Ti_3O_{10}$, in this case using a triple perovskite block from $CaTiO_3$ ($b \simeq 27$ Å, see Table 3). However, the use of a *C*-face centring to generate the second triple perovskite block within the unit cell gave an arrangement of atoms not directly conforming to any space group with the correct cell dimensions. Therefore atoms of the second perovskite block were positioned with respect to those of the first block such that the intergrown NaCl structure between the blocks is the same as in $Ca_3Ti_2O_7$. This layer arrangement is shown in Fig. 2. The TiO_6 octahedra tilt cooperatively across the intergrown layer such that their adjacent apical O atoms lie in rows along [100]. Tilts are alternate along [001] in the CaO layer. The tilt pattern within the perovskite layers still conforms to that in $CaTiO_3$ and the resulting space group is *Pcab* (No. 61).

Neutron diffraction patterns were not analysed for absences for the $n = 3$ compounds because the $Ca_4Ti_3O_{10}$ pattern contains moderately strong peaks from the $Ca_3Ti_2O_7$ impurity, and the $Ca_{3.6}Sr_{0.4}Ti_3O_{10}$ pattern has *a* and *c* too nearly equal for determination of absences (Table 3). The space group *Pcab* was however confirmed by the success of later refinements (§4.2).

CBED investigation of $Ca_4Ti_3O_{10}$ was restricted to [010] and neighbouring zones by preferred cleavage perpendicular to the long axis. Good [010] zone patterns were, however, obtained with both (*h*0*l*) and

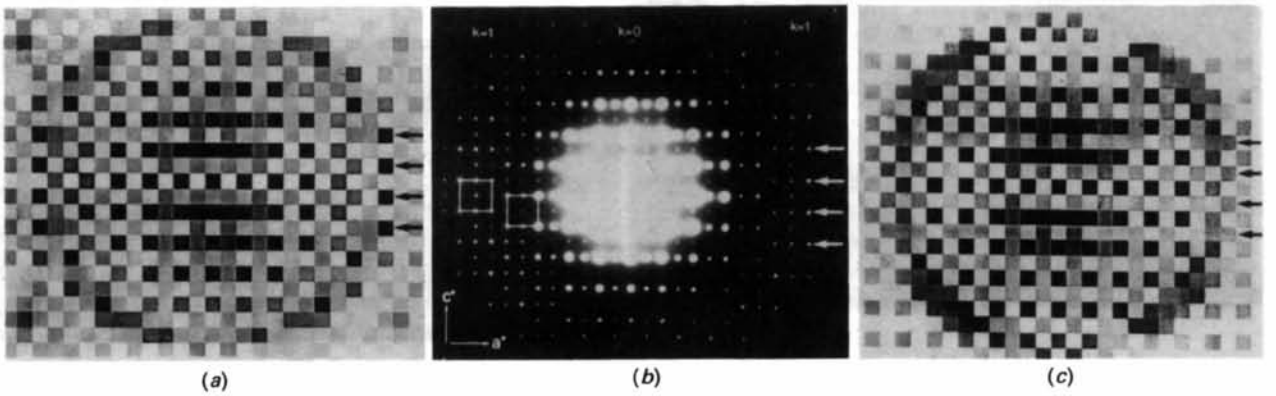

Fig. 5. Multi-slice simulated [010] patterns from $Ca_4Ti_3O_{10}$ for the space groups (*a*) *Pcab* (neutron determined atom positions), (*b*) Fig. 4(*a*) for direct comparison and (*c*) *Acam* (atoms shifted to higher-symmetry positions). Arrows indicate the (11,1,$\bar{3}$), (11,1,$\bar{1}$), (11,1,1) and (11,1,3) reflections.

Table 2. [010] *zone observations from* $Ca_4Ti_3O_{10}$

Symmetry	*h*0*l*	*pmg*
	*h*1*l*	*pgg*
Absences	*h*0*l*	$l = 2n$
	*h*1*l*	$l = 2n + 1$ ($h = 2n + 1$)

(*h*1*l*) reflections. Fig. 3(*a*) shows a complete pattern, exhibiting zero-layer (*h*0*l*) symmetry *pmg*, with $l = 2n + 1$ rows absent and dynamic extinction bands through the (*h*00) *h*-odd reflections. In addition, the first-order Laue zone (*h*1*l*) has the symmetry *pgg*, since extinction bands are found through the (*h*10) and (01*l*) reflections (see detail in Fig. 3*b*).

To distinguish between pure glide bands (*G*) and glide–screw bands (*GS*) along the (*h*00) row, the crystal was rotated about the *a** axis. In Fig. 3(*c*) the [041] zone pattern shows complete extinction of the (*h*00) *h*-odd reflections proving the existence of a 2_1 parallel to the *a** axis and the '*a*' glide plane (identified in Fig. 3*a*). This combined symmetry (summarized by the layer-group symbol *pbaa*'2_1') proves the space-group class *mmm*, and allows space groups Nos. 52, 54, 56, 60, 61 and 64 (Goodman, Matheson & White, 1991).

The point pattern from the [010] zone (Fig. 4*a*) has the following reflection conditions: *h*0*l*: $l = 2n$; *h*1*l*: $l = 2n + 1$ ($h = 2n + 1$); giving *hkl*: $k + l = 2n$ *i.e.* *A*-centring, and in the absence of further data one would conclude that *Cmca* (No. 64) is the correct space group in conflict with the derived structure and the neutron diffraction results.

Multi-slice calculations in *Pcab* and *Cmca* were run to simulate the [010] electron diffraction intensities. Atomic coordinates determined by neutron diffraction were used for *Pcab* and for *Cmca* these atomic positions were modified to fit the higher symmetry. Results of the simulations are shown in Figs. 5(*a*) and 5(*c*) along with the observed pattern (Fig. 5*b*).

The *Pcab* coordinates clearly reproduce the observed (*h*1*l*) intensities more closely than do those for *Cmca*. In particular the higher-order Laue zone intensities for the reflections (*h*,11,1), with $h = 1, 3, -1, -3$.

The above calculations demonstrate that the centring deduced from the CBED patterns is a pseudo-centring only, arising from the operations of three perpendicular glide planes. As indicated in Table 2, the out-of-zone absences which arise in *Pcab* on some special positions, resemble those for a cell centred on all faces ($h + k$, $k + l$, $l + h = 2n$). All of the Ti and half of the Ca atoms are on or are close to face-centred positions. The remaining atoms, particularly the O atoms, occupy positions which should destroy the effective centring in diffraction. This effect can be seen in Fig. 4(*b*) ([101] zone) where the *k*-odd reflections along the (0*k*0) row are completely extinguished due to the presence of the 2_1 operator parallel to *b**, but along the (*hkh*) rows ($h \neq 0$) all reflections have some intensity.

In conclusion, it is noted that in the *mmm* class, this pseudo-centring can only occur in the space groups *Pcab* and *Pccn* (No. 56).

4. Structure refinement

Rietveld refinements of the neutron diffraction data were carried out using the program *LHPM*1 (Hill & Howard, 1986), a modified Wiles & Young (1981) program. A Voigt peak shape corrected for asymmetry by the sum of five peaks method (Howard, 1982) was used. For each compound, the counter zero, four polynomial background coefficients, peak half-widths *U*, *V*, *W* (Gaussian) and *K* (Lorentzian), and an asymmetry parameter were the refined instrument parameters. Where impurity phases were present, only their scale factors were refined and the algorithm of Hill & Howard (1987) was used to determine their relative abundance. The scattering lengths $-0{\cdot}3438$, $0{\cdot}702$ and $0{\cdot}5805 \times 10^{-12}$ cm were used for Ti, Sr and O respectively. The value $0{\cdot}469 \times 10^{-12}$ cm was used for Ca in preference to the currently accepted value of $0{\cdot}490 \times 10^{-12}$ cm (Sears, 1984), as refinements in our laboratory of the occupancy of Ca sites in Ca-containing compounds have consistently indicated this to be a better value.

4.1. $n = 2$

The $Sr_3Ti_2O_7$ structure of Ruddlesden & Popper (1958) was refined in space group *I*4/*mmm*. Refined coordinates, lattice parameters, thermal parameters and final *R* values are given in Table 3. There is good agreement with the coordinates of Ruddlesden & Popper (1958), the greatest discrepancy being for O(2) which is displaced by 0·11 Å along [001]. The impurity $SrTiO_3$ was found to represent 4·8 (1)% of the sample by mass.

Refinement of $Ca_3Ti_2O_7$ in $Ccm2_1$ with the tilted starting model converged quickly to $R_{wp} = 5{\cdot}94\%$, $S = 1{\cdot}92$ and $R_B = 3{\cdot}77\%$. Analysis of differences suggested slight [010] preferred orientation, not unexpected in a structure layered on (0*k*0) planes. When a March model (Dollase, 1986) preferred orientation parameter was included in the refinement, the refinement converged to give $R_{wp} = 4{\cdot}99\%$, $S = 1{\cdot}35$ and $R_B = 1{\cdot}37\%$. The Rietveld plot is shown in Fig. 6 and illustrates excellent agreement with the data. Refined unit-cell parameters, atomic coordinates and thermal parameters are given in Table 3. High correlation was observed between the parameters $z_{O(3)}$ and $z_{O(4)}$ (96%), and $z_{O(1)}$ and $z_{O(2)}$ (93%). Hence the constraints $x_{O(3)} = x_{O(4)} - \frac{1}{2}$, $z_{O(3)} = \frac{1}{2} - z_{O(4)}$ and $z_{O(1)} = -z_{O(2)}$ were imposed with no resultant degra-

Table 3. *Structural parameters*

$Sr_3Ti_2O_7$
I4/mmm (139), R_{wp} = 8·27%, R_B = 1·54%, S = 3·40, $a = b$ = 3·9026 (1), c = 20·3716 (4) Å, 78 reflections

	x	y	z	B(Å^2)
Sr(1)	½	½	0	0·16 (9)
Sr(2)	½	½	0·1842 (1)	0·54 (7)
Ti	0	0	0·0964 (3)	0·48 (8)
O(1)	0	0	0	0·64 (11)
O(2)	0	0	0·1934 (2)	0·42 (9)
O(3)	0	½	0·0961 (1)	0·44 (4)

$Ca_3Ti_2O_7$
*Ccm*2$_1$ (36), R_{wp} = 4·99%, R_B = 1·37%, S = 1·35, a = 5·4172 (1), b = 19·5169 (4), c = 5·4234 (1) Å, 200 reflections

Ca(1)	0·2517 (9)	0	0·0290 (12)	0·62 (8)
Ca(2)	0·7410 (5)	0·1876 (2)	0·4747 (8)	0·74 (6)
Ti	0·2491 (9)	0·0989 (2)	¼	0·24 (5)
O(1)	0·8124 (6)	0	−0·0132 (3)*	0·58 (7)
O(2)	0·6958 (5)	0·1972 (1)	0·0132 (3)*	0·77 (5)
O(3)	0·5378 (2)*	0·0860 (1)	0·2883 (2)*	0·52 (2)*
O(4)	0·0378 (2)*	0·1099 (1)	0·2117 (2)*	0·52 (2)*

$Ca_4Ti_3O_{10}$
Pcab (61), R_{wp} = 5·16%, R_B = 1·53%, S = 1·39, a = 5·4083 (1), b = 27·1432 (4), c = 5·4337 (1) Å, 441 reflections

Ca(1)	0·5038 (8)	0·0693 (3)	0·4665 (9)	0·43 (9)
Ca(2)	−0·0079 (5)	0·2053 (2)	0·0238 (12)	0·74 (10)
Ti(1)	0	0	¼	0·06 (6)*
Ti(2)	0·4973 (13)	0·1426 (2)	0	0·06 (6)*
O(1)	0·4332 (5)	0·0708 (2)	0·0142 (3)*	0·51 (8)
O(2)	0·5548 (8)	0·2118 (2)	−0·0142 (3)*	0·74 (9)
O(3)	0·7125 (8)	0·1321 (1)	0·7115 (2)*	0·47 (5)*
O(4)	0·2875 (7)	0·1499 (1)	0·2885 (2)*	0·47 (5)*
O(5)	0·2099 (7)	−0·0100 (2)	0·7885 (2)*	0·60 (7)

$Ca_{3.6}Sr_{0.4}Ti_3O_{10}$
Pcab (61), R_{wp} = 5·81%, R_B = 1·55%, S = 1·84, a = 5·4409 (2), b = 27·2727 (7), c = 5·4415 (2) Å, 447 reflections

Ca(1)†	0·9982 (9)	0·0690 (3)	0·9814 (15)	0·65 (12)
Ca(2)	−0·0093 (13)	0·2051 (2)	0·0136 (21)	0·79 (12)
Ti(1)	0	0	¼	0·33 (6)*
Ti(2)	0·4954 (17)	0·1432 (2)	0	0·33 (6)*
O(1)	0·4427 (7)	0·0716 (2)	0·0103 (5)*	0·79 (12)
O(2)	0·5494 (10)	0·2118 (3)	−0·0103 (5)*	1·12 (11)
O(3)	0·7193 (11)	0·1338 (2)	0·7189 (4)*	0·84 (6)*
O(4)	0·2813 (10)	0·1488 (1)	0·2811 (4)*	0·84 (6)*
O(5)	0·2161 (10)	−0·0088 (2)	0·7811 (4)*	1·06 (9)

* Constrained parameters.
† Site of Sr substitution.

dation of the fit. The structure is illustrated in Fig. 7. The O(1) atoms are at the hinging y-axis apices of the octahedra in the middle of each perovskite block whilst O(2) atoms are at the apices in the intergrown CaO. The O(3) site of $Sr_3Ti_2O_7$ which defines the octahedral mid-planes has become the two sites O(3) and O(4) in $Ca_3Ti_2O_7$.

4.2. $n = 3$

Refinement of $Ca_4Ti_3O_{10}$ in *Pcab* with the tilted starting model was immediately successful. The Rietveld plot is given in Fig. 8 and again shows very good agreement between the calculated and observed profiles. Impurity peaks from the 10·4 (1) mass % of $Ca_3Ti_2O_7$ in the sample are also well described by the calculation. Refined unit-cell constants, atom coordinates, thermal parameters and agreement indices are given in Table 3. The z coordinates of O(1) and O(2), and also those of O(3), O(4) and O(5) were highly correlated and no degradation of the fit was observed when the following constraints were imposed; $z_{O(1)} = -z_{O(2)}$, $-z_{O(3)} = z_{O(4)} = z_{O(5)} - \frac{1}{2}$. Fig. 9 is a view of the structure along [101]. O(1) and O(2) are as before but there are now three types of oxygen sites defining mid-planes of octahedra. O(3) and O(4) are in the octahedra adjacent to the interface between blocks and are equivalent to O(3) and O(4) of $Ca_3Ti_2O_7$. The mid-planes of octahedra in the centre of the triple perovskite blocks are defined by one site; O(5). The tilt motif within the perovskite blocks is the same as in $Ca_3Ti_2O_7$ (and $CaTiO_3$), with tilts intermediate between $Ca_3Ti_2O_7$ and $CaTiO_3$. There are two distinct types of TiO_6 octahedra, those in the middle of the perovskite blocks (type 1) and those at the edge of the blocks (type 2).

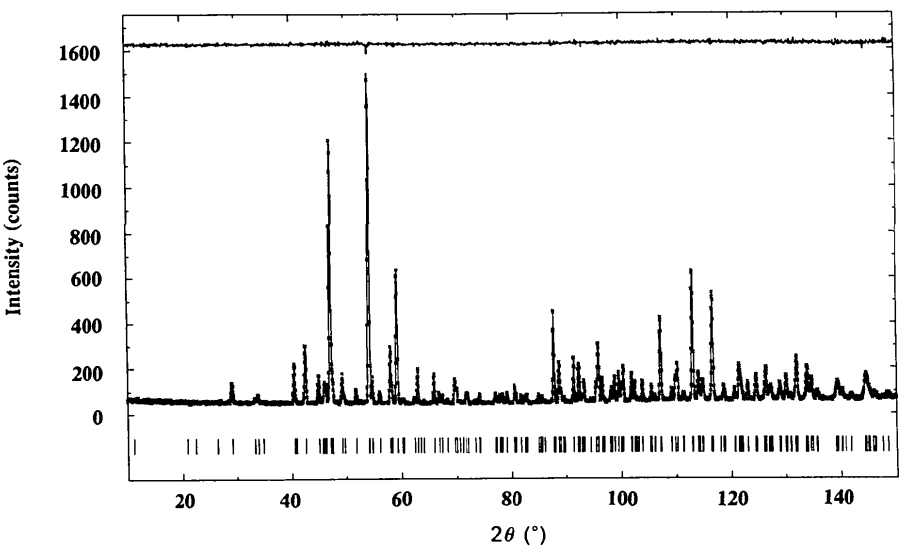

Fig. 6. Rietveld refinement result for $Ca_3Ti_2O_7$. Data points are given as crosses, the calculated profile as a solid line through them and a difference plot on the same scale is shown as a solid line above. Vertical bars show all allowed reflections of the space group *Ccm*2$_1$.

The sample of nominal composition $Ca_{3.4}Sr_{0.6}Ti_3O_{10}$ has a neutron diffraction pattern similar to that of $Ca_4Ti_3O_{10}$. Consequently, the $Ca_4Ti_3O_{10}$ structure was used as a starting model. The agreement before refinement of coordinates was $R_{wp} = 11{\cdot}93\%$, $S = 7{\cdot}66$ and $R_B = 11{\cdot}43\%$, indicating that the addition of this small amount of Sr has a significant influence on the structure. Refinement of atom coordinates, thermal parameters, occupancies of the Ca sites and a scale factor for the ~3% of $(Ca/Sr)_3Ti_2O_7$ present resulted in a considerable improvement to $R_{wp} = 5{\cdot}81\%$, $S = 1{\cdot}84$ and $R_B = 1{\cdot}55\%$. The same atom positional constraints were used as for $Ca_4Ti_3O_{10}$. Refined crystal structure parameters are given in Table 3. The Ca site occupancies indicated that the larger Sr atoms substitute preferentially on the Ca(1) site, within the perovskite layers. The Ca(2) site (between perovskite layers) remains fully Ca occupied. This is consistent with the fact that mean Ca(1)—O distances are greater than Ca(2)—O distances in $Ca_4Ti_3O_{10}$. A composition of $Ca_{3.6}Sr_{0.4}Ti_3O_{10}$ is indicated by the refined occupancies. The $(Ca/Sr)_3Ti_2O_7$ impurity is hence probably richer in Sr than the major phase but too little is present for this to be determined.

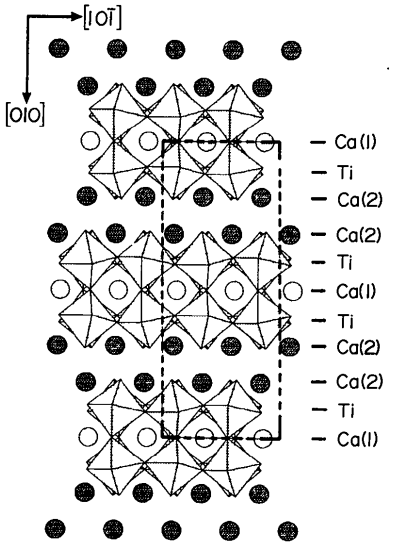

Fig. 7. A [101] projection of the $Ca_3Ti_2O_7$ structure showing the tilt pattern of corner-linked TiO_6 octahedra. The cations are labelled and the unit cell shown in outline.

5. Discussion

A most striking feature of perovskite structures is their flexibility with respect to relative cation size. This is achieved by tilting of the BX_6 octahedra which are the most rigid parts of the structures. Often the B cations are non-central in their octahedra, even if these are untilted. To simplify discussions of relationships between perovskite-related structures, BX_6 octahedra are often considered completely rigid. In reality, however, tilting and/or non-central B cations lead to slight distortions of the octahedra.

This polysomatic series of structures with $n = 2$ and $n = 3$ as well as Koopmans *et al.* (1983) coordinates for $CaTiO_3$ ($n = \infty$) provides an excellent opportunity for quantitative examination of octahedral tilting, non-centricity of B cations in octahedra and distortions to octahedra for different values of n. In addition, the refinement of $Ca_{3.6}Sr_{0.4}Ti_3O_{10}$ allows the influence of doping with a larger A cation to be examined. Throughout the

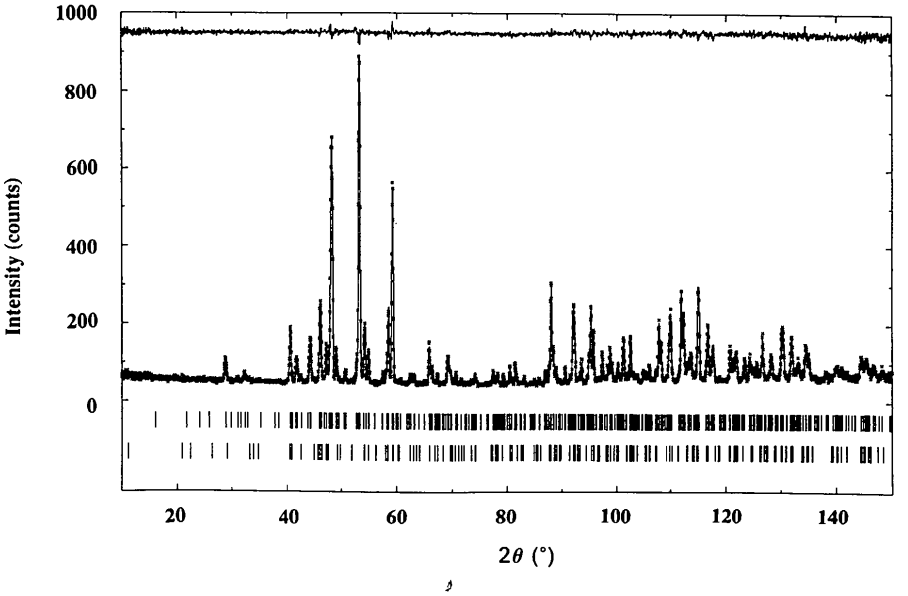

Fig. 8. Rietveld refinement results for $Ca_4Ti_3O_{10}$. Data points are given as crosses, the calculated and difference profiles as solid lines. Reflection markers show line positions for $Ca_4Ti_3O_{10}$ (*Pcab*) top and $Ca_3Ti_2O_7$ ($Ccm2_1$) bottom.

following, use will be made of the calculated bond lengths.*

5.1. *Octahedral tilt measurement*

Tilting of BX_6 octahedra has received various treatments. In particular, Glazer (1972) describes a system of classification of tilt patterns based on positive and negative rotations about the three cubic sub-cell axes a_c, b_c and c_c for perovskite structures with unit cells no bigger in any direction than $2a_c$. In Glazer's notation, $CaTiO_3$ ($n = \infty$) conforms to the $a^- b^+ a^-$ tilt pattern. Since the sense of the rotations is unchanged in the $Ca_3Ti_2O_7$ and $Ca_4Ti_3O_{10}$ structures, if the treatment were extended to include perovskite blocks within Ruddlesden–Popper phases, the structures described here also conform to $a^- b^+ a^-$ (except $Sr_3Ti_2O_7$ which is $a^0 b^0 c^0$). To quantify the tilts is more difficult since rotational operators about the cubic axes belong to a non-abelian group making the final result dependent on the order in which the rotations are carried out.

O'Keefe & Hyde (1977) describe a method for quantifying tilts of octahedra which, for $CaTiO_3$, involves calculating the angle of tilt (φ) about the cubic [111] axis. To keep the octahedra regular, a second tilt (ψ) of the octahedron and the primary axes is required.

* See deposition footnote.

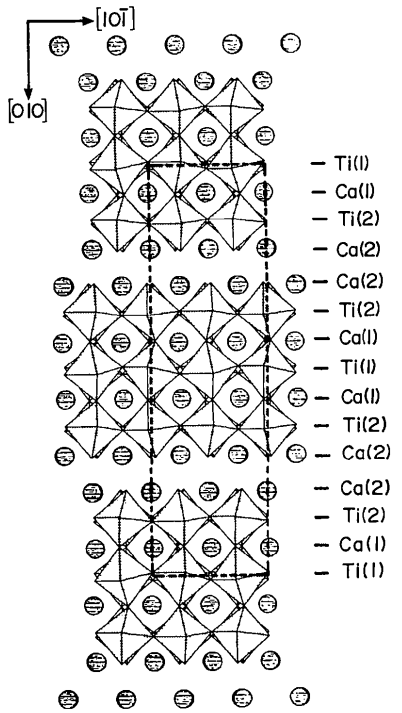

Fig. 9. A [101] projection of the $Ca_4Ti_3O_{10}$ structure showing the tilt pattern of the TiO_6 octahedra. Cation sites are labelled and the unit cell shown in outline.

An exact description is provided by Megaw (1973). Tilts leading to orthorhombic structures of the $CaTiO_3$ type are combinations of a tilt about a fourfold axis of the (undistorted) octahedra (here called η_1) and a tilt about a twofold axis of the octahedra (η_2). Both are defined in Fig. 10. Since the angles of tilt about axes of the octahedra are used rather than directions in the cubic sub-cell, an unambiguous structure description results. In the special case where $\eta_2 = 2^{1/2}\eta_1$, the diad tilt is equivalent to tilts of equal magnitude to η_1 about two further tetrad axes. The resultant is equivalent to a tilt about a triad axis of the octahedron, similar to the method of O'Keefe & Hyde. Values of η_1 and η_2 for the structures reported here are given in Table 4 with the equations for their calculation. Because the octahedra are distorted, each is the mean of two slightly different values.

We are aware of only one analysis of tilted octahedra in Ruddlesden–Popper phases (Aleksandrov, 1987). This group-theoretical analysis of space groups arising from all possible tilt patterns in $n = 1$

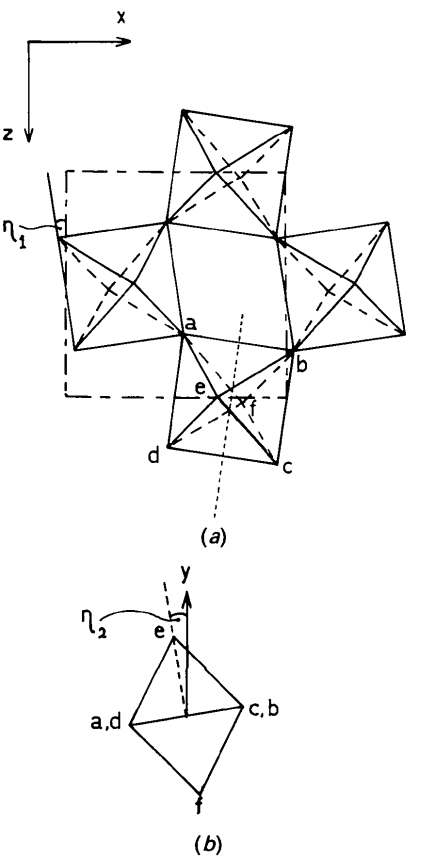

Fig. 10. (*a*) An [010] projection of one layer of tilted TiO_6 octahedra showing the tilt angle η_1 about a pseudo-tetrad axis of the octahedra. (*b*) A projection of one octahedron along the dotted axis in (*a*), showing the tilt about a pseudo-diad axis η_2 (*y* drawn vertical for clarity).

Table 4. *Tilt angles, displacement and distortion indices*

Phase	η_1 (°)	η_2 (°)	S_d (%)	S_φ (%)	D_d (%)	D_φ (%)
$Sr_3Ti_2O_7$	0	0	0·4	0·2	0·3	0·1
$Ca_3Ti_2O_7$	8·6	9·7	0·3	0·8	0·6	0·3
$Ca_4Ti_3O_{10}$						
Type 1	9·0	11·2	0·2	0·2	0·5	0·2
Type 2	8·6	10·1	1·2	1·2	0·6	0·4
$CaTiO_3$	8·9	11·7	0·2	0·5	0·6	0·3
$Ca_{3.6}Sr_{0.4}Ti_3O_{10}$						
Type 1	7·5	10·2	0·7	0·3	0·5	0·6
Type 2	7·2	8·5	1·4	1·3	0·5	0·4

For atoms a, b, c, d, e, f defined in Fig. 10:

$\eta_1 = 45 - \tan^{-1}[(z_a - z_c)c/(x_a - x_c)a]$,
$\eta_2 = \sin^{-1}\{(y_d - y_a)b/[(x_d - x_a)^2a^2 + (y_d - y_a)^2b^2 + (z_d - z_a)^2c^2]^{1/2}\}$,
$S_d = \sum_{i=1}^{6}[|(\widehat{Ti—O})_{mean} - (\widehat{Ti—O})_{i,obs}|/(\widehat{Ti—O})_{mean}] \times 100$,
$S_\varphi = \sum_{i=1}^{12}[|(\widehat{OTiO})_{mean} - (\widehat{OTiO})_{i,obs}|/(\widehat{OTiO})_{mean}] \times 100$,
$D_d = \sum_{i=1}^{12}[|(\widehat{O—O})_{mean} - (\widehat{O—O})_{i,obs}|/(\widehat{Ti—O})_{mean}] \times 100$,
$D_\varphi = \sum_{i=1}^{12}[|(\widehat{OO_iO})_{mean} - 90°|/90°] \times 100$.

structures produces many more possibilities, few of which are realized in known structures.

5.2. *Variation of tilt with n*

From Table 4 it is clear that the equality $\eta_2 = 2^{1/2}\eta_1$ is approximately true for $CaTiO_3$ but not for the other structures. Both η_1 and η_2 increase as n, η_2 being the more sensitive. Tilts of octahedra occur in perovskites to stabilize the structure by reduction of the size of the 12-coordinated A cation sites to match the A cation size. In the Ruddlesden–Popper series $Ca_{n+1}Ti_nO_{3n+1}$, 12-coordinated A sites (perovskite blocks) and 9-coordinated A sites (CaO intergrowths) are present in the ratio $n-1:2$. Clearly an $n = 1$ member of the series (Ca_2TiO_4) has no 12-coordinated A site and is hence very unstable in this system. From this it can be understood why no observations of Ca_2TiO_4 have been reported.

Octahedral tilts are known to be temperature and pressure sensitive. For example, $SrTiO_3$ in which the octahedra are untilted at room temperature becomes tetragonal below 103 K by tilting about a tetrad axis. This occurs by a soft-mode transition (Shirane & Yamada, 1969) and a maximum tilt angle of $\eta_1 = 1{\cdot}3°$ is attained near to 0 K. The decreasing tilt angles observed in the CaO–TiO_2 system for the sequence $n = \infty, 3, 2$ are consistent with the observed decrease in melting temperature in this sequence (Roth, 1958).

5.3. *Variation of tilt with* Sr *addition*

Examination of the mean Ca—O bond lengths for $Ca_4Ti_3O_{10}$ shows the Ca(1) site to be slightly larger. It is therefore not surprising that larger Sr cations substitute preferentially onto these sites. The effect on tilt angles is large in $Ca_{3.6}Sr_{0.4}Ti_3O_{10}$ (Table 4). This fairly low level of substitution reduces η_1 and η_2 by more than a degree each. In a companion publication (Hawkins & White, 1991), X-ray powder diffraction and high-resolution electron microscopy are used to examine the $Ca_{n+1}Ti_nO_{3n+1}$–$Sr_{n+1}Ti_nO_{3n+1}$ solid-solution series. Here it is shown that at sufficiently high levels of Sr addition, the lattice parameters become tetragonal. Therefore η_2 becomes zero but η_1 may remain non-zero, in which case the space group predicted by the algorithm in §3.1 and 3.2 is *Ccma* (No. 64). The postulated structure is orthorhombic despite the tetragonal unit cell because the fourfold axis is destroyed by the intergrown CaO layers.

5.4. *Off-centre* Ti *atoms*

In all the compounds studied here, the Ti atoms are non-central in the oxygen octahedra. $Sr_3Ti_2O_7$ has the Ti displaced along the c axis with respect to the octahedral mid-planes by 0·01 Å. The Ca compounds also show this displacement (along the orthorhombic b axis) but with much greater magnitude. They also show small displacements of Ti laterally towards O(3) and O(4) atoms in the $n = 2$ structure and the type 2 octahedra of the $n = 3$ structure. Type 1 octahedra of the $n = 3$ structure have Ti constrained by symmetry to be central in distorted octahedra. To quantify these complex displacements the indices S_d and S_φ are given in Table 4. They are the mean percentage deviations from the mean Ti—O bond lengths and angles respectively.

Clearly the displacement of Ti in type 2 octahedra of $n = 3$ structures is greater than in type 1 octahedra. Doping with Sr apparently accentuates this effect as well as increasing S_d and S_φ in the type 1 octahedra of $Ca_{3.6}Sr_{0.4}Ti_3O_{10}$. In all cases, the displacement along [010] is much greater than in other directions.

5.5. *Distortions of octahedra*

TiO_6 octahedra in $Sr_3Ti_2O_7$ have square-pyramidal halves of unequal heights [*i.e.* O(2)—O(3) distances are longer than O(3)—O(3) and O(1)—O(3)]. That half shared with the intergrown CaO layer is slightly relaxed (0·02 Å) towards it whilst the other half is nearly regular [*i.e.* O(3)—O(3) is nearly equal to O(1)—O(3)].

In $Ca_3Ti_2O_7$ and the type 2 octahedra of $Ca_4Ti_3O_{10}$ and $Ca_{3.6}Sr_{0.4}Ti_3O_{10}$ there are three broad types of distortion. Their halves are of slightly unequal height as above. They are doubly 'bent', with apical O atoms which project to points on the mid-plane displaced along both [100] and [001] from centre. Thirdly, their mid-planes are rectangular, not square as in a regular octahedron. The type 1 octahedra of $Ca_4Ti_3O_{10}$ and $Ca_{3.6}Sr_{0.4}Ti_3O_{10}$ have a centre of symmetry and are hence more regular.

To compare such complexly distorted shapes, it becomes necessary to invoke some quantitative

measure of the distortion. To do so we use the indices D_d and D_φ which are the percentage mean deviations of octahedron bond lengths and angles respectively from their mean values. They are given in Table 4 along with values calculated for $CaTiO_3$ ($n = \infty$). The mean distortions are fairly small, never greater than 1%. They are significantly greater in the CaO–TiO_2 compounds than in $Sr_3Ti_2O_7$ and there are no significant trends in the series $n = 2, 3, \infty$. However, the two types of octahedra in $n = 3$ structures appear to have a different degree of distortion especially with respect to angles (D_φ).

6. Concluding remarks

A procedure for predicting the space group of members of this series from the structure of the $n = \infty$ member is outlined in §3.1. and 3.2. It can be extended to indicate that the most likely space group for all n-even members is $Ccm2_1$ and for n-odd members is $Pcab$. This procedure should find general application in the solution of all such layered structures from known $n = \infty$ end members. Where our analysis has overlapped with that, for $n = 1$, of Aleksandrov (1987), the two approaches are in agreement.

The combined use of neutron powder diffraction and CBED in the solution of such structures is to be recommended. It should however, be noted that a space group could not be successfully allocated from the available CBED patterns without pattern simulations which relied on the neutron determined atomic positions.

Support under the National Research Fellowship scheme is gratefully acknowledged by EHK. Many thanks to Professor P. E. Fielding of the University of New England for preparation of the $Sr_3Ti_2O_7$ sample.

References

ALEKSANDROV, K. S. (1987). *Sov. Phys. Crystallogr.* **32**, 551–558.
DOLLASE, W. A. (1986). *J. Appl. Cryst.* **19**, 267–372.
DRY'S, M. & TRZEBIATOWSKI, W. (1957). *Rocz. Chem.* **31**, 489–496.
GLAZER, A. M. (1972). *Acta Cryst.* B**28**, 3384–3392.
GOODMAN, P., MATHESON, S. & WHITE, T. J. (1991). In preparation.
HAWKINS, K. D. & WHITE, T. J. (1991). In preparation.
HILL, R. J. & HOWARD, C. J. (1986). Australian Atomic Energy Commission Report No. M112. AAEC, Lucas Heights Research Laboratories, New South Wales, Australia.
HILL, R. J. & HOWARD, C. J. (1987). *J. Appl. Cryst.* **20**, 467–474.
HOWARD, C. J. (1982). *J. Appl. Cryst.* **15**, 615–620.
HOWARD, C. J., BALL, C. J., DAVIS, R. L. & ELCOMBE, M. M. (1983). *Aust. J. Phys.* **36**, 507–518.
KOOPMANS, H. J. A., VAN DE VELDE, G. M. H. & GELLINGS, P. J. (1983). *Acta Cryst.* C**39**, 1323–1325.
KWESTROO, W. & PAPING H. A. M. (1959). *J. Am. Ceram. Soc.* **42**, 293 299.
LUKASZEWICZ, K. (1959). *Rocz. Chem.* **33**, 239–242.
MEGAW, H. D. (1973). *Crystal Structures: A Working Approach.* Philadelphia: W. B. Saunders.
O'KEEFE, M. & HYDE, B. G. (1977). *Acta Cryst.* B**33**, 3802–3813.
ROTH, R. S. (1958). *J. Res. Natl Bur. Stand.* **61**, 437–440.
RUDDLESDEN, S. N. & POPPER, P. (1957). *Acta Cryst.* **10**, 538–539.
RUDDLESDEN, S. N. & POPPER, P. (1958). *Acta Cryst.* **11**, 54–55.
SEARS, V. J. (1984). Atomic Energy of Canada Ltd Report No. 8490. AECL, Chalk River, Canada.
SHIRANE, G. & YAMADA, Y. (1969). *Phys. Rev.* **177**, 858–863.
TILLOCA, G. & PEREZ Y JORBA, M. (1964). *Rev. Hautes Temp. Refract.* **1**, 331.
WILES, D. B. & YOUNG, R. A. (1981). *J. Appl. Cryst.* **14**, 149–151.

Acta Cryst. (1991). B**47**, 314–325

Determination of the Modulated Structure of the Inorganic Misfit Layer Compound $(PbS)_{1.18}TiS_2$

BY SANDER VAN SMAALEN, AUKE MEETSMA, GERRIT A. WIEGERS AND JAN L. DE BOER

Laboratory of Inorganic Chemistry, Materials Science Center, University of Groningen, Nijenborgh 16, *NL* 9747 *AG Groningen, The Netherlands*

(*Received* 15 *October* 1990; *accepted* 28 *November* 1990)

Abstract

Single-crystal X-ray diffraction results (Mo $K\bar{\alpha}$ radiation, $\lambda = 0.71073$ Å) are presented for the inorganic misfit layer compound titanium sulfide $(PbS)_{1.18}TiS_2$ which can be described as a two-component structure. The first subsystem (TiS_2, $\nu = 1$) has space-group symmetry $C2_1/m$, and a basic structure unit cell given by $a_{11} = 3.409$ (1), $a_{12} = 5.880$ (2), $a_{13} = 11.760$ (2) Å and $\alpha_1 = 95.29$ (2)°. The modulation wavevector is $\mathbf{q}^1 = \mathbf{a}^*_{21} = \alpha\mathbf{a}^*_{11}$, with $\alpha = 0.5878$ (3). Its subsystem superspace group is $P^{C2_1/m}_{1\ 1}$ (α, 0, 0). The second subsystem (PbS, $\nu = 2$) has space group $C2/m$ and a basic structure unit cell given by $a_{21} = 5.800$ (2), $a_{22} = 5.881$ (2), $a_{23} = 11.759$ (2) Å and $\alpha_2 = 95.27$ (2)°. The modulation wavevector is $\mathbf{q}^2 = \mathbf{a}^*_{11}$. The subsystem superspace group is $P^{C2/m}_{s\ 1}$ (α^{-1}, 0, 0). The relation between the

0108-7681/91/030314-12$03.00